Pergamon

0042-6989(95)00225-1

Vision Res., Vol. 36, No. 8, pp. 1067–1079, 1996

Printed in Great Britain
0042-6989/96 $15.00 + 0.00

Images of Cone Photoreceptors in the Living Human Eye

DONALD T. MILLER,*‡ DAVID R. WILLIAMS,† G. MICHAEL MORRIS,* JUNZHONG LIANG†

Received 22 March 1995; in revised form 7 August 1995

Though the photoreceptor mosaic has been imaged through the intact optics of the eyes of several species, it has not been clear whether individual photoreceptors can be resolved in the living human eye. We have constructed a high-resolution fundus camera and have resolved cones with a spacing as small as 3.5 μm in single images of the fundus. The high contrast of these images implies that almost all the light returning from the retina at this wavelength (555 nm) has passed through the apertures of foveal cones. The average power spectra of our retinal images show that it is possible to recover spatial frequencies as high as 150 c/deg in eyes with normal optical quality, a conclusion that was confirmed with estimates of the optical quality of these eyes obtained with a Hartmann–Shack wavefront sensor. These results emphasize the superiority of the eye's optics over the spatial sampling limits of the retina when the eye's optical quality is optimized. They also show that it would be possible to routinely resolve retinal structures as small as photoreceptors in the normal living eye if its aberrations could be corrected.

Fovea Cones Fundus imaging Resolution Point-spread function

INTRODUCTION

Blurring by the eye's optics limits both the finest patterns that can be imaged on the retina and the smallest retinal features that can be imaged outside the living eye. Helmholtz (1873) and numerous authors since (Snyder & Miller, 1977; Yellott, 1982, 1983; Williams, 1985, 1992; Land, 1990) have pointed to a rough match between this optical limit and the limit imposed by the grain of the foveal cone mosaic. That is, the highest spatial frequency passed by the eye's optics in bright light is roughly equal to the Nyquist limit of the foveal cone mosaic. The notion underlying this match is that evolution has engineered the eye's optics to give the retina access only to the low spatial frequencies it adequately samples while removing the spatial frequencies above the Nyquist limit that would alias. Despite this apparent match at the foveal center, it is well known that, under laboratory conditions in which the eye is carefully refracted, the optics are superior to the retinal grain everywhere else in the visual field (Jennings & Charman, 1981; Navarro *et al.*, 1993; Williams *et al.*, in press). A match between the optics and sampling seems to be the exception rather than the rule across the animal kingdom in compound eyes (Snyder, 1979; Wehner, 1981) as well as in vertebrate eyes (Snyder *et al.*, 1986, 1990). Snyder *et al.* argued that the optical cutoff almost always exceeds the Nyquist limit because the benefit of superior optics in increased contrast sensitivity at subNyquist spatial frequencies outweighs the increased risk of aliasing.

This relationship between optics and retinal grain has interesting implications for experiments in which the eye's optics are used in reverse to view the living retina. For example, if the optics were good enough to pass spatial frequencies as high as the cone sampling frequency, which is twice the Nyquist frequency, it should be possible to resolve them in the intact eye (Land & Snyder, 1985). In several snake species as well as the cane toad, single photoreceptors were resolved through the intact optics by capitalizing on their large photoreceptors and good optics (Land & Snyder, 1985; Zwick *et al.*, 1995; Jagger, 1985). For four vertebrate species including humans, Snyder *et al.* (1986, 1990) showed that the optical cutoff frequency is roughly twice the Nyquist limit of the photoreceptor mosaic in at least some portion of the retina, leading to the prediction that individual photoreceptors could be potentially resolved through the intact optics of these species. Specifically, Snyder *et al.* (1986, 1990) pointed out that human cones at 10 deg from the foveal center have a sampling frequency of about 26 c/deg which is potentially low enough for the mosaic to be resolved through the intact optics, assuming a diffraction-limited 2 mm pupil.

Despite these theoretical predictions, there has been no compelling evidence that receptors can be resolved in an

*The Institute of Optics, University of Rochester, Rochester NY 14627, U.S.A.
†Center for Visual Science, University of Rochester, Rochester, NY 14627, U.S.A.
‡To whom all correspondence should be addressed [*Email* miller@cvs.rochester.edu].

image of the living human retina. Current fundus cameras including scanning laser ophthalmoscopes, while well-suited to capture macroscopic retinal features, do not resolve retinal structures as small as single cells. We have constructed a high-resolution fundus camera to establish the highest spatial frequencies that can be recovered from the living retina. We show here that when the pupil is large and defocus and astigmatism are carefully corrected, the cone mosaic near the foveal center can be seen in some eyes through the intact optics. We also describe independent estimates of the optical quality of these eyes, showing that it is indeed high enough to resolve the cone mosaic.

FUNDUS IMAGING EXPERIMENTS

Methods

A schematic of the high-resolution fundus camera is shown in Fig. 1. An argon-pumped dye laser, S, illuminated a small patch of retina with 555 nm light. The beam from the laser passed through an acousto-optic modulator, AOM, that generated 4 msec retinal exposures, short enough to eliminate motion blur due to eye movements. The beam then passed through two adjacent counter-rotating phase diffusers (Lowenthal & Joyeux, 1971) that scattered the light in a broad range of directions, making the field spatially incoherent. The rotating diffusers were conjugate with a field stop, FS, and the retina of the observer. The field stop limited the field size to 6.8 min arc. Adjacent to the field stop was a fixation target. The artificial pupil AP_1 was conjugate with the observer's natural pupil and controlled the size of the beam entering the observer's eye. The subject's astigmatism and defocus were carefully corrected with trial lenses. The total laser power incident on the cornea for the six subjects ranged from 0.1 to 0.5 mW. For the 4 msec exposures used, the laser power at the cornea was 5–27 times below the ANSI Z-136.1 exposure limit.

The light reflecting out of the eye passed through an artificial pupil, AP_2, that was conjugate with the observer's natural pupil, which was typically dilated. The exit pupil typically was either 5 or 6 mm in the plane of the natural pupil. The light then reflected from mirrors M1 and M2. M2 was mounted on a computer-controlled galvanometer that was designed to quickly rotate between two different orientations in <3 msec. When synchronized with two 4 msec exposures, the quick rotation of M2 permitted aerial images of essentially the same patch of retina to form at two separate locations on a cooled, single frame CCD camera (Photometrics Series 200 system, Thomson TH7895B chip). This technique permitted measurement of photopigment bleaching in photoreceptors caused by the first of the two 4 msec exposures.

Six subjects were used in the experiment, ranging in age from 24 to 40 years. Typically, the pupil was dilated and accommodation reduced with tropicamide (1%) or cyclopentolate hydrochloride (1%). Images of the subject's retina were collected at retinal locations ranging from the central fovea out to 2.5 deg.

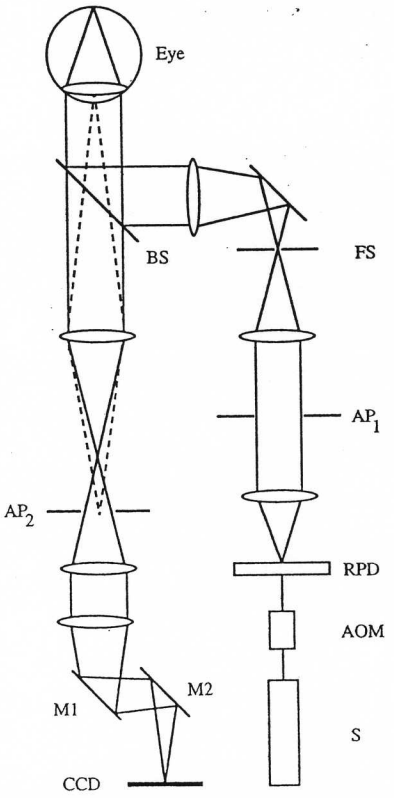

FIGURE 1. Schematic diagram of the high-resolution fundus camera used to collect images of the retina through the intact optics of the living human eye. See text for description.

Results

Figure 2 shows images collected using the fundus camera on subjects JL and MM at 0.5 and 1.25 deg eccentricity, i.e., from the foveal center. The images from JL are among the best of 30 images collected at each retinal location. For MM, they are among the best of 12 images collected at each retinal location. Each subject's accommodation was paralyzed and pupil dilated using cyclopentolate hydrochloride (1%). Defocus and astigmatism were corrected with trial lenses. The exit pupil was 6 mm. The contrast of the images is lower for MM than that for JL. Nonetheless, arrays of bright spots can be seen in all four images. Though the intensity of these spots varies, they form a fairly regular packing arrangement similar in spacing and shape to the cone mosaics seen in light micrographs at roughly the same eccentricities (from Curcio *et al.*, 1990).

Several observations ensure that the bright spots found in the images were not caused by the speckle that results when spatially coherent light reflects from a rough object. First, the rotating phase diffusers in the fundus camera made the retinal illumination highly spatially incoherent. The speckle size (or equivalently the spatial coherence length) of the illumination at the retina was calculated to be 0.39 min arc (1.88 μm) for a 6 mm pupil and an illumination wavelength of 555 nm (Dainty, 1984). This speckle size is well below the spacing of the bright spots observed in our images, which was never smaller than

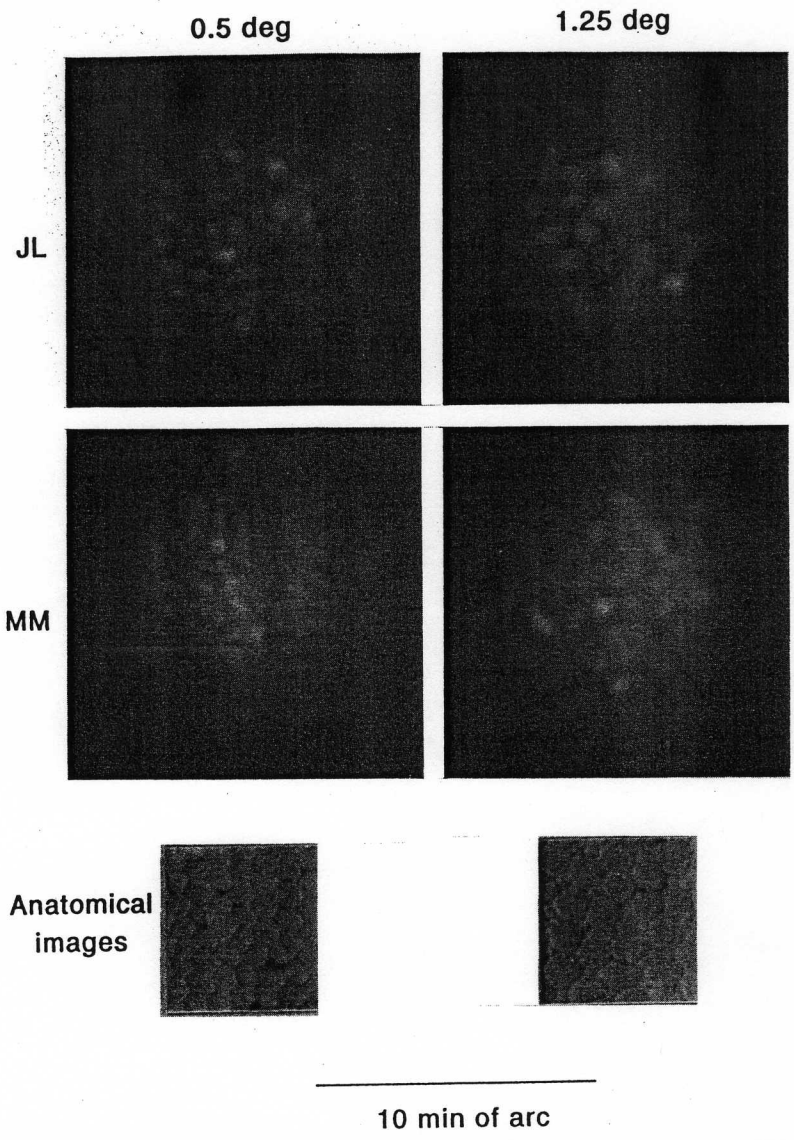

FIGURE 2. Several of the best images collected using the fundus camera on subjects JL and MM at 0.5 and 1.25 deg eccentricity. The four images contain illuminated retinal patches 6.8 min arc in diameter. Two light micrographs of the cone mosaic at roughly the same eccentricities (0.42 and 1.4 deg) are also shown for comparison.

0.64 min. In addition, the contrast of the speckle was calculated based on the total displacement of the rotating diffusers for a 4 msec exposure and the width of the diffraction-limited point spread function (PSF) of the fundus camera at the rotating diffusers. The speckle contrast was defined as the standard deviation of the speckle irradiance divided by the mean irradiance. A conservative estimate of the speckle's contrast at the retina is 1.25% (Lowenthal & Joyeux, 1971), too low to be responsible for the higher contrast, bright spots we observed.

Furthermore, the size of speckle should be inversely proportional to the diameter of the exit pupil (Dainty, 1984), but we found that the size of the bright spots was independent of pupil size. Figure 3 shows two images collected at 2.5 deg eccentricity using the 3 and 6 mm exit pupils for subject JL. Accommodation was paralyzed and the pupil dilated using cyclopentolate hydrochloride (1%). The patches of retina are different in the two images due to eye movements between exposures. The spacing of the bright spots is essentially the same in the two images, about 1.08 min arc. Had the bright spots been speckled, the size of the bright spots using the 3 mm pupil would have been twice as large as that observed with the 6 mm pupil. Results obtained at retinal eccentricities of 0.5 and 1.25 deg support the same conclusion.

As illustrated in Fig. 3, movements of the eye between flashes introduced displacements which, because of the small field size we generally used, made it difficult to determine how repeatable our retinal images actually were. We obtained a few observations with a larger, 13 min arc illuminating field. In this case, it was sometimes possible to identify the same spatial pattern of bright spots from exposure to exposure. To investigate repeatability unconfounded by eye movements, we performed experiments in which two images of the same retinal location were collected 7 msec apart, which was

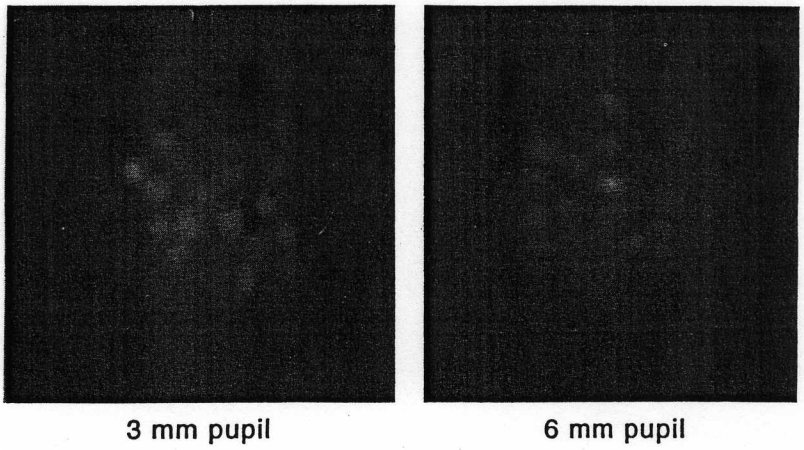

FIGURE 3. Two images collected at 2.5 deg eccentricity using a 3 and 6 mm exit pupil. The patches of retina are different in the two images due to eye movements between exposures. The spacing of the bright spots in both images is about 1.08 min arc.

too short to allow substantial movement of the retina. Figure 4 shows a typical pair of images from JL at 0.5 deg eccentricity with a 6.8 min arc field. Accommodation was paralyzed with cyclopentolate hydrochloride (1%). The exit pupil was 6 mm. The second image always revealed the same spatial pattern as the first except that the irradiance was about 10% greater due to photopigment bleaching by the first flash. This increase was not accompanied by a measurable increase in the contrast of the bright spots, a point we will return to in the Discussion. The increase in irradiance in the second image shows that at least some of the light forming these images has traversed the photopigment layer.

The individual retinal images collected on some observers never showed clear evidence for the array of bright spots. However, in these cases, we were able to extract evidence for the arrays from the power spectra of the retinal images. Yellott (1982, 1983) showed that the power spectrum of the cone mosaic of excised retinas has power concentrated in a ring about the origin. The radius of this ring corresponds to the cone sampling frequency, which is the reciprocal of cone spacing. Artal and Navarro (1989) proposed a clever method to measure cone spacing in the living eye, using spatially coherent light to illuminate the retina, that is similar to stellar speckle interferometry, a method to recover information about celestial objects that overcomes blurring by atmospheric turbulence (Dainty, 1984). They predicted the average power spectrum of many short-exposure retinal images would preserve information about the periodicity of the photoreceptor mosaic that is lost in the noise in individual images, thus revealing Yellott's ring.

Average power spectra were computed from images collected at eccentricities ranging from zero to 2.5 deg.

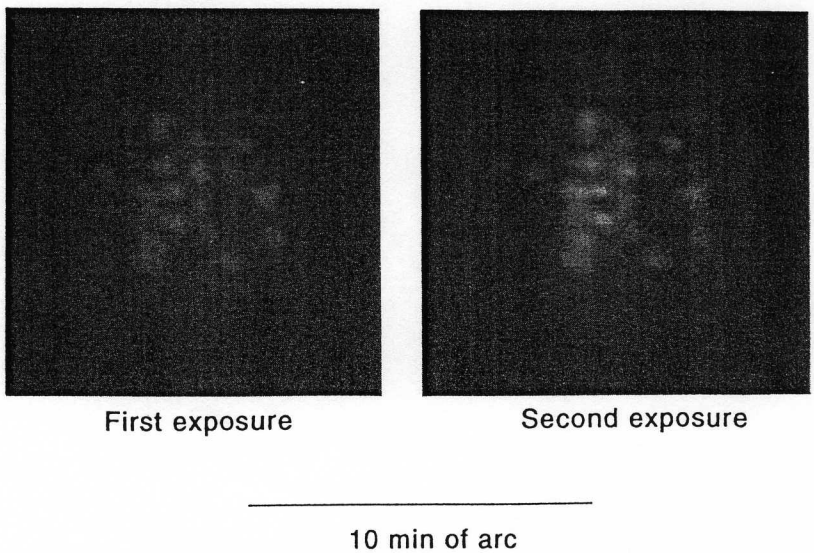

FIGURE 4. Typical set of images collected 7 msec apart from JL at 0.5 deg eccentricity. The second exposure is essentially identical to the first except that it is around 10% brighter due to photopigment bleaching by the first flash.

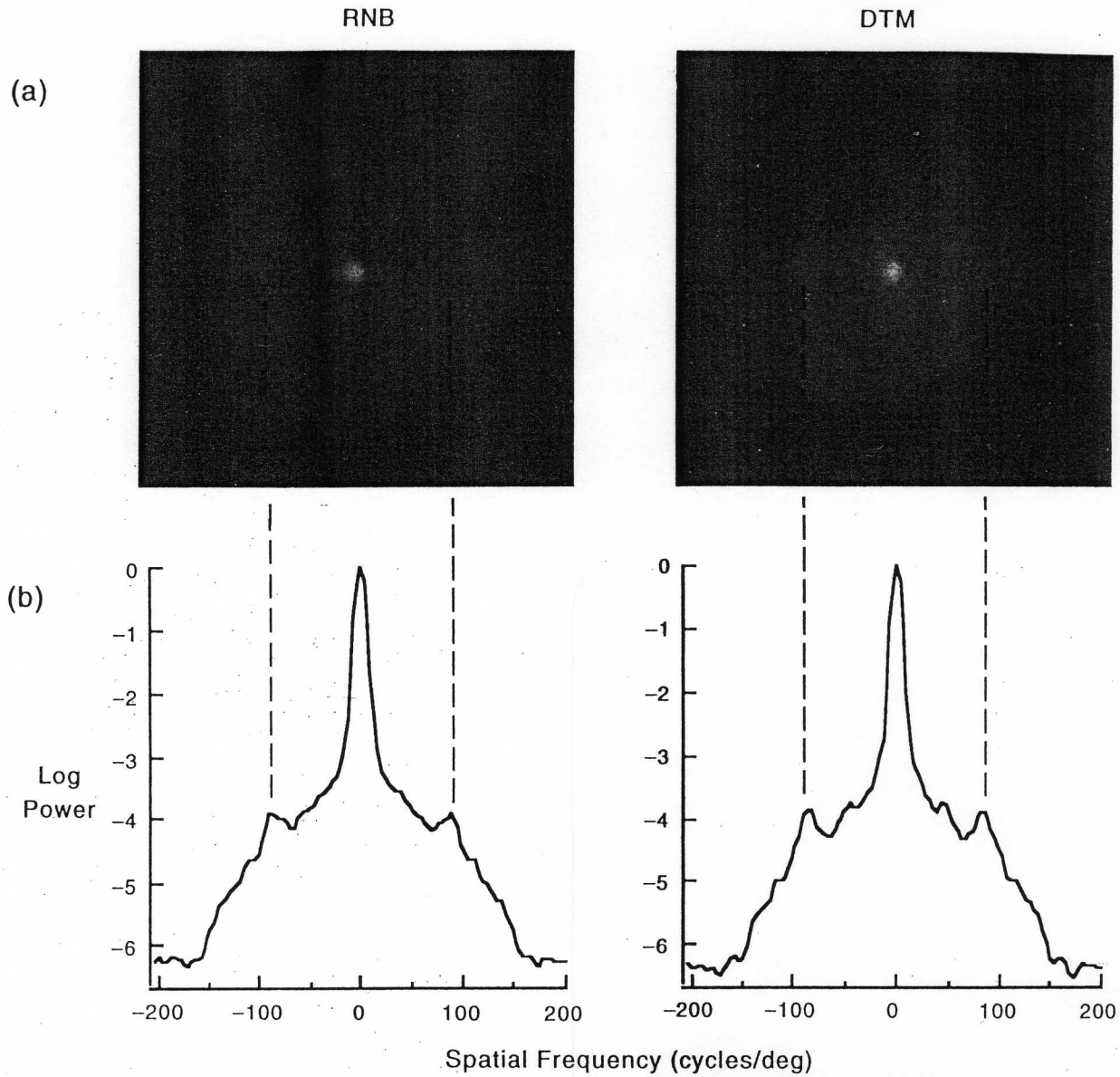

FIGURE 5. (a) Logarithmic gray-scale images of the average power spectra obtained by averaging the power spectra of 15 and 12 retinal images collected at 0.5 deg from the central fovea on subjects RNB and DM, respectively. A faint elliptical ring is visible in both images. (b) Horizontal cross sections through the center of the power spectra also show the rings.

Figure 5 shows images of the average power spectra obtained by averaging the power spectra of 15 and 12 retinal images collected at 0.5 deg from the central fovea on subjects RNB and DM, respectively. The exit pupil was 5 mm. RNB's and DM's pupils were dilated using cyclopentolate hydrochloride (1%) and tropicamide (1%), respectively. Both power spectra in Fig. 5(a) reveal Yellott's ring as Artal and Navarro had predicted. A faint elliptical ring is visible in both images, which reveals the cone mosaic that could not be clearly discerned in individual images in these subjects. For subject RNB the cone mosaic is apparently disorderly enough even at 0.5 deg eccentricity to have a Yellott ring type spectrum. In DM's power spectrum, on the other hand, the ring is broken up into six regions with relatively more power suggesting the cones are arranged in a more regular array with hexagonal packing. In Fig. 5(b) horizontal cross sections through the center of the power spectra also show the rings, which appear as a cusp on a steep slope of declining power that extends all the way to the diffraction limit. The rings correspond to sampling frequencies of 89 c/deg or a cone spacing of 0.67 min arc in subject RNB and 85 c/deg or a cone spacing of 0.71 min arc in subject DM.

Figure 6 compares the reciprocal of the average ring radius with anatomical and psychophysical measures of cone spacing. Depending on the observer, either 12, 15, or 30 images were collected on each of six observers at various retinal eccentricities near the fovea. The data points correspond to the reciprocal of the average radius of the rings, except for JL's estimates that were directly measured from the retinal images. Because the slope of the eye's MTF causes a slight decrease in the ring's diameter, using the ring's diameter probably slightly

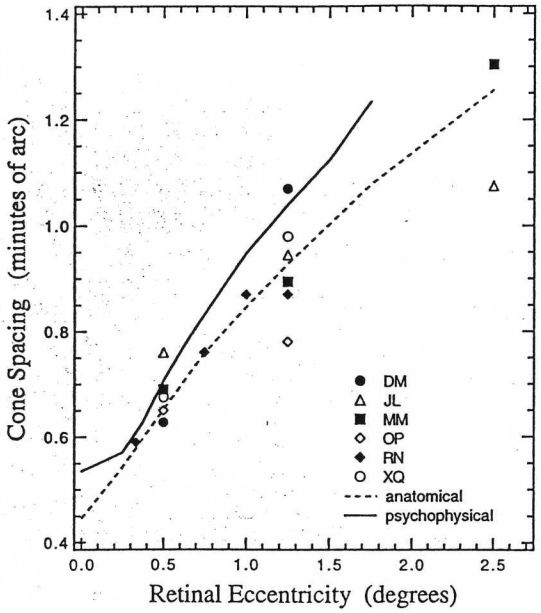

FIGURE 6. Estimates of cone spacing obtained from retinal images at various retinal eccentricities compared with anatomical and psychophysical estimates of cone spacing for six observers. Depending on the observer, either 12, 15, or 30 images were collected on each of six observers at various retinal eccentricities near the fovea. The data points correspond to the reciprocal of the average radius of the rings, except for JL's estimates that were directly measured from the retinal images. The dashed line shows anatomical estimates of cone spacing from Curcio *et al.* (1990). The solid line shows estimates of cone spacing based on psychophysical observations of aliasing with interference fringes (Williams, 1988).

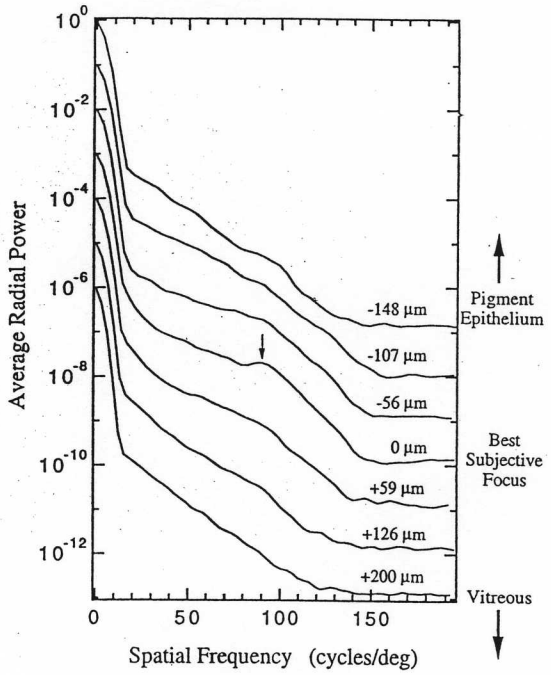

FIGURE 7. Radial-average cross sections of average power spectra computed from images collected at seven different focal planes in the retina. The images were collected from subject DM at 0.5 deg eccentricity using a 5 mm exit pupil. Each of the curves corresponds to a particular plane in the retina whose relative position to the plane of best subjective focus is given by the number above each curve, which are in units of microns. Retinal landmarks are displayed to the right of the plot, indicating the relative position of each curve to the pigment epithelium, plane of best subjective focus, and vitreous. Only the middle curve (corresponding to the plane of best subjective focus) contains a significant hump, which is indicated by an arrow. This hump indicates the presence of a ring at this location in the power spectrum and corresponds to a spatial frequency of 88 c/deg.

overestimates cone spacing. The dashed line shows anatomical estimates of cone spacing from Curcio *et al.* (1990). The solid line shows estimates of cone spacing based on psychophysical observations of aliasing with interference fringes (Williams, 1988). The rough agreement between the data sets supports the view that the bright spots correspond to individual cones.

Even in those eyes in which bright spots are visible in individual images, they are not seen in every image, possibly due to defocus from small drifts in accommodation. Correspondingly, the rings in the power spectra were very sensitive to defocus. Figure 7 shows average power spectra computed from images collected at seven different focal planes in the retina in approx. 56 μm (0.15 diopters) steps. The power spectra show the radial average. That is, they have been averaged across all orientations. The images were collected from subject DM at 0.5 deg eccentricity using a 5 mm exit pupil. Accommodation was not paralyzed in this case. The axial location of the plane is specified in microns relative to the plane of best subjective focus. The latter plane was established using sphere and cylinder trial lenses to optimize the subjective image quality of a fixation target at the same optical distance as the CCD camera. Retinal landmarks are displayed to the right of the plot, indicating the position of the pigment epithelium and vitreous relative to each focal plane. We assume here that the plane of best subjective focus corresponds to the cone inner segments. Only the middle curve corresponding to the plane of best subjective focus contains a significant cusp, at a spatial frequency of 88 c/deg. The focal plane producing the clearest ring in the power spectrum agreed within measurement error (0.15 diopters) with the plane of best subjective focus. Since the best subjective focus corresponds to the cone layer, these results suggest that the arrays of bright spots are produced by the receptors.

SIMULATION OF FUNDUS IMAGING

Methods

We next sought independent evidence that the optical quality of the particular eyes we had examined was indeed good enough to resolve cones so close to the fovea. The wave aberration of four of the six subjects' eyes (DM, JL, OP, and XQ) was measured with a Hartmann–Shack wavefront sensor (Liang & Williams, 1995). The method was similar to that described by Liang *et al.* (1994) and a detailed description will be published elsewhere. The eye's wave aberration was measured by sensing the wavefront at the pupil produced by the retinal reflection of a focused light spot on the retina. The squared modulus of the Fourier transform of the pupil

function, containing the wave aberration, gives the optical PSF of the eye. We modeled the retinal imaging process by convolving this PSF with a simulated cone mosaic to determine whether the mosaic could be recovered.

The cone mosaic was simulated by taking cone locations from micrographs of excised human retina (Curcio *et al.*, 1990) at four retinal eccentricities (foveal center, 0.42, 1.4, and 2.2 deg). A two-dimensional Gaussian function was placed at each cone and rod location, representing the expected light profile exiting the photoreceptor. The full width half maximum (FWHM) of the Gaussian function was taken to be 0.48 times the diameter of the cone or rod inner segment. Inner segment diameters were measured directly from the micrographs. The value of 0.48 was taken from psychophysical estimates of the cone aperture using a distortion product technique (MacLeod *et al.*, 1992; Chen *et al.*, 1993). The volume under each Gaussian function was proportional to the area of the inner segment of the cone or rod.

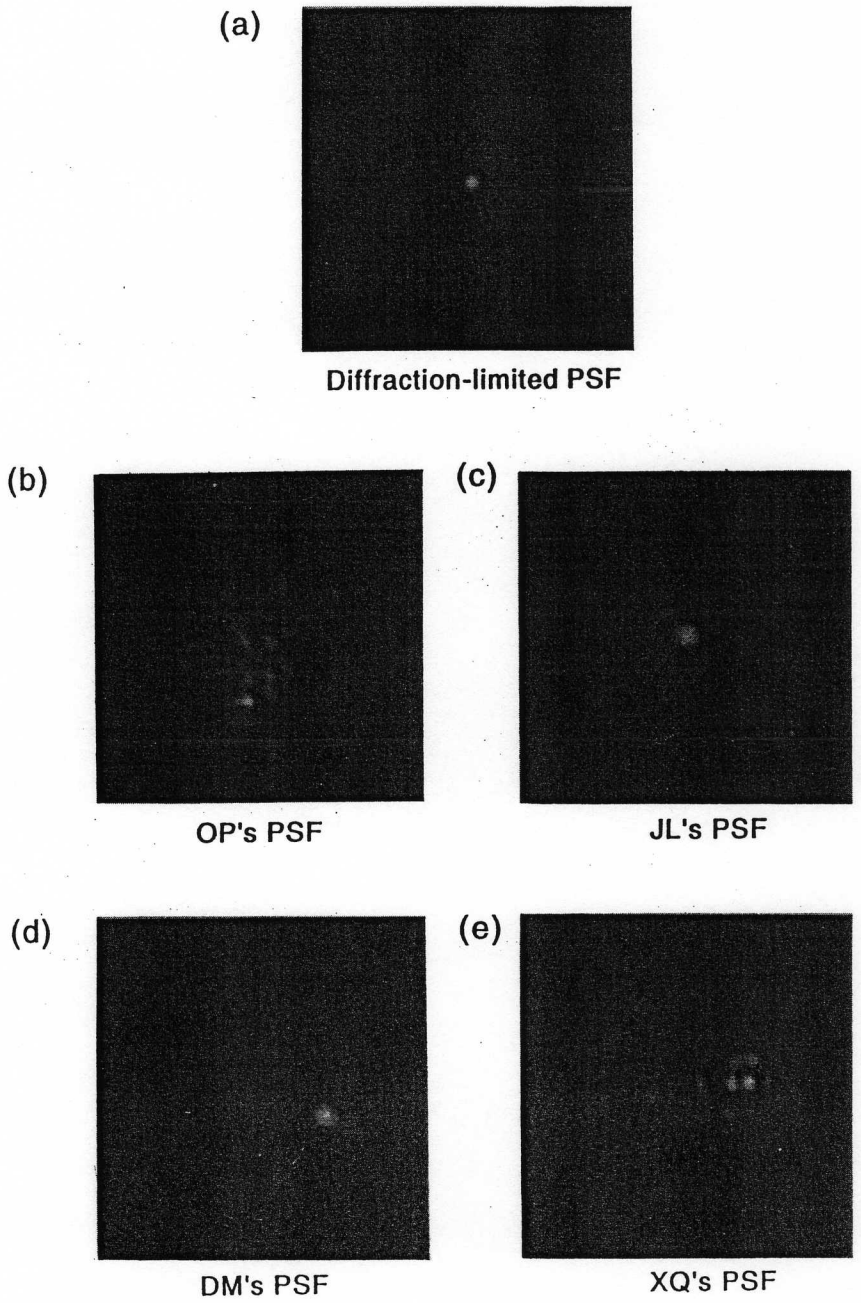

FIGURE 8. (a) Diffraction-limited PSF and measured PSFs from four subjects, (b) OP, (c) JL, (d) DM, and (e) XQ are shown for a 6 mm exit pupil and an illumination wavelength of 555 nm. The PSFs are corrected for defocus and astigmatism.

Results

The PSFs obtained using a Hartmann–Shack wavefront sensor from subjects DM, JL, OP, and XQ, as well as the diffraction-limited PSF, are shown in Fig. 8 for a 6 mm exit pupil and an illumination wavelength of 555 nm. The PSFs are corrected for defocus and astigmatism, and their Strehl ratios are 0.083, 0.092, 0.079, and 0.091 for OP, JL, DM, and XQ, respectively.

The PSF for JL's eye has the most central compact shape of the four subjects which provides unusually good imagery. It is in his eye that the most convincing images of the cone mosaic were obtained. The FWHM of JL's PSF is about 2.6 μm (0.54 min arc) and is broadened slightly from the diffraction-limited PSF (FWHM = 1.6 μm) mainly by spherical aberration. The form of the PSF for subjects OP and XQ results from many higher order Zernike aberrations that give it an extended, complex shape not well suited for imaging. DM's irregular PSF is primarily caused by third order Zernike aberrations, which include coma. The large individual differences in optical quality seen here, even when defocus and astigmatism are corrected, confirm large individual differences in MTF reported by Walsh *et al.* (1984).

Figure 9 shows the results of the simulations for observer JL at the four retinal eccentricities (foveal center, 0.42, 1.4, and 2.2 deg). All images correspond to square retinal regions 26 μm wide. The exit pupil was 6 mm and the illumination wavelength was 555 nm. The left-most column shows the simulated mosaics. The middle column shows the simulated mosaics convolved with the diffraction-limited point spread function. Though these images are blurred in comparison to the simulated photoreceptor mosaics, individual cones and

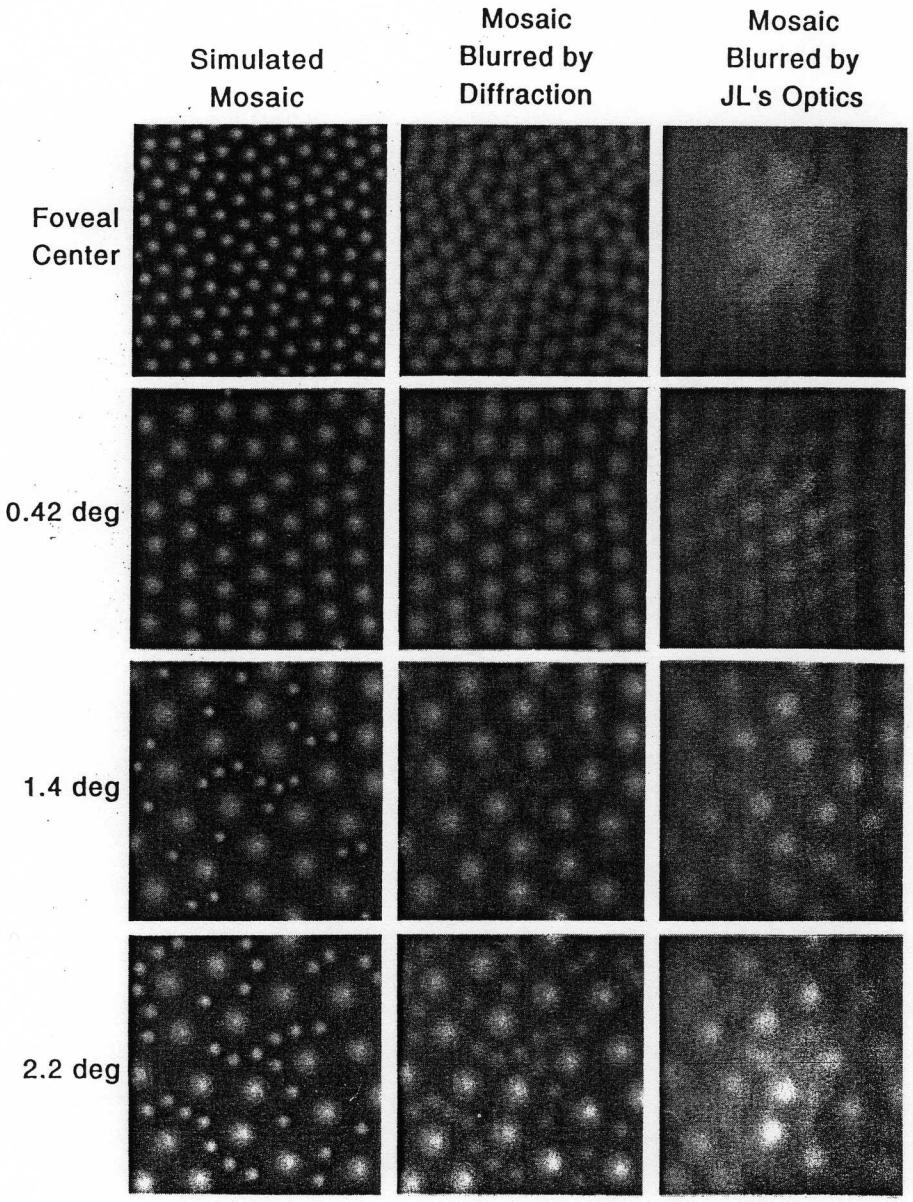

FIGURE 9. Results of convolving the diffraction-limited PSF and JL's PSF with simulated photoreceptor mosaics at the foveal center, 0.42, 1.4, and 2.2 deg eccentricity. The mosaics are square retinal regions 26 μm wide. The exit pupil was 6 mm and the illumination wavelength was 555 nm.

rods are still clearly distinguishable at all four retinal eccentricities. This shows that microscopic spatial structure could easily be resolved if the aberrations of the eye were corrected.

The right-most column in Fig. 9 shows the convolution of the simulated photoreceptor mosaic with JL's PSF. The simulation predicts that JL's optics are not good enough to resolve the cones at the foveal center. This agrees well with our inability to resolve cones there in his eye using the fundus camera. The simulation also shows that the cone spacing has increased enough at eccentricities 0.42, 1.4, and 2.2 deg so that single cones, but not the rods, can be resolved at all three locations. This also agrees well with experiments on his eye, since we can see the arrays of bright spots at similar eccentricities in our experiments. The average contrast of the cones predicted by the simulation at 0.42, 1.4, and 2.2 deg eccentricity is about 25%, which is reasonably close to the value we typically observed in our experiments. For example, in our clearest images collected, the contrast between the bright spots and the darker spaces between them was about 31%. From these results we conclude that the optical quality of JL's eye is indeed good enough to resolve cones.

Because the Stiles–Crawford effect of the first kind (SCE I) reduces the effective pupil size of the eye and could change image quality in fundus images, the simulation was repeated using JL's PSF with the SCE I included. The directional sensitivity of the SCE I was expressed as

$$\eta = 10^{-\rho r^2}, \quad (1)$$

where r is the radial distance from the center of the natural pupil. ρ is the shape factor and was set to $0.08\ \text{mm}^{-2}$, a value close to that measured by van Blokland for light scattering from the human fundus (van Blokland, 1986). The results of the simulation using the SCE I were very similar to those shown in Fig. 9, suggesting that the SCE I does not have an important effect on retinal image contrast in this case.

When the simulations were repeated with the PSFs of DM and OP, which were considerably broader than that of JL, it was generally not possible to resolve the simulated mosaics in individual images. This is consistent with the fact that we could not obtain convincing evidence for the cone mosaic in individual images obtained on these eyes, and were forced to used the technique of averaging power spectra.

DISCUSSION

In eyes that have demonstrably superior optics, we have been able to resolve arrays of bright spots in individual images obtained with the high-resolution fundus camera. We reject speckle as an explanation for the spots, and provide two lines of evidence that these spots correspond to the cone mosaic. First, their spacing agrees well with that of cones as a function of eccentricity. Second, Yellott's ring was seen only at the subjective focal plane, which corresponds to the receptor layer and probably the cone inner segments. This shows that it is possible to recover microscopic structure from fundus images. These results have implications for the nature of the fundus reflection, the optical quality of the eye and its relation to retinal sampling, and the future prospects for high-resolution imaging, discussed in turn below.

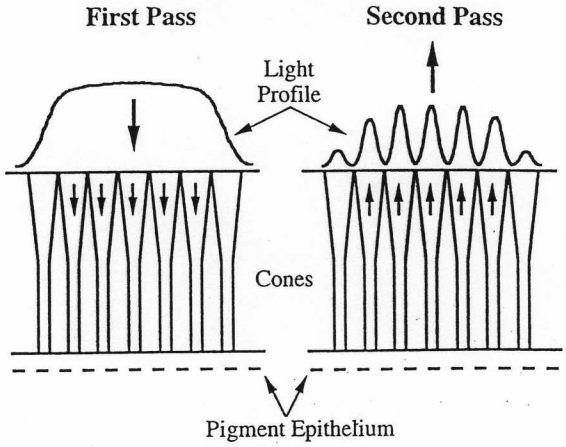

FIGURE 10. Schematic cross sections of cones showing the probable path of light through the retina that would generate the arrays of bright spots shown in Fig. 2. The first pass (left schematic cross section) shows the coupling of the incident light into the cones. The second pass (right schematic cross section) shows the coupled light emerging from the cone apertures, which produces a modulated intensity pattern consisting of an array of distinguishable bright spots.

Implications for the nature of the fundus reflection

Figure 10 shows a provisional description of the light path through the cones that could produce the array of bright spots. The directional properties of light returning from the fundus (Krauskopf, 1965; van Blokland & van Norren, 1986; Gorrand & Delori, 1995; Burns *et al.*, 1995) shows that the much of the light has been guided in the receptors. In the first pass, some of the incident light is coupled into and propagates down the cones. In the second pass, the coupled light is reflected back and emerges from the cone apertures producing a modulated intensity pattern consisting of an array of bright spots. The layer or layers behind the receptors that reflect most of the light back is uncertain though it is likely to lie very close to the scleral end of the outer segments, such as in the pigment epithelium (van Blokland & van Norren, 1986; Gorrand & Delori, 1995). There may also be a contribution from other sites within the receptor, such as the junction between inner and outer segments.

The best images of the cone mosaic, obtained on observer JL, have remarkably high contrasts for so fine a periodic structure, sometimes as high as 31%. The choice of a small patch of illuminated retina in our camera, typically only 6.8 min arc, improved the image contrast. When the illumination field approaches the dimensions of the eye's PSF, the contrast reduction caused by the tails of the PSF is reduced. This is because, when the small illuminated patch is convolved with the PSF, much of the tail of the PSF falls outside the illuminated patch where it

cannot reduce contrast. In simulations in which JL's optical PSF was convolved with illuminated retinal patches of various sizes, it was found that a 6.8 min arc illumination diameter increases the contrast in the image by roughly a factor of two over that obtained when a very large section of the retina is illuminated.

Nonetheless, the eye's optics inevitably blur the images we obtain so that the actual contrast of the cone mosaic must be considerably higher than the contrast of our images. Our simulations suggested that the mosaic contrast must be close to 100%, so that the regions between the bright spots return very little light. We varied the mosaic contrast in the simulation by changing the FWHM of the Gaussian light profile exiting each receptor. We found that if we assumed a FWHM much broader than about half the diameter of the receptor inner segment, the simulation produced a mosaic image contrast too low to be consistent with JL's images. For example, if the FWHM was chosen to equal the inner segment diameter, the simulation predicted that cones are unresolvable at any of the four retinal eccentricities, even in the diffraction-limited case.

The high contrast of the cone mosaic suggests that almost all the light in our images passes through a rather narrow exit pupil for each cone. Presumably this light is guided by the receptors. Our observations of photopigment bleaching also support this view. The fact that the irradiance of the second of two successive images is greater than the first shows that some of the light in our images has traversed the photopigment layer. However, we found that the percentage increase in photopigment transmittance measured at the center of each bright spot was not significantly higher than the percentage increase in the dark spaces between bright spots. This suggests that the light in the bright and dark regions of the image has passed through the same amount of the photopigment. If the light we observed in the dark regions between bright spots were light passing between the receptors, we would have expected to find less photopigment there. Our use of two successive flashes each of which bleached a fraction of the photopigment did not optimize the reflectance difference before and after bleaching. It would be of some interest to repeat these experiments under optimal conditions.

Any unguided light is apparently reflected back toward the pupil with much less efficiency. This could occur if the site of the reflection back toward the pupil were different for guided than for unguided light. The unguided light may also be selected against if it is more broadly back scattered than the guided light, the latter being directed back toward the pupil. The high contrast of the mosaic leaves no room for important contributions from prereceptoral layers in imaging this part of the fundus at this wavelength. Because of the high magnification of the fundus camera, the corneal reflex produces a uniform veil in our retinal images of negligible irradiance. Most of the retinal locations where we observed cones lay on the slope of the foveal pit, so that the slope of the internal limiting membrane would have been too steep to have introduced a specular reflection in our images. One implication of the high contrast of the cone mosaic is that the relatively low estimates of photopigment density obtained with retinal densitometry must be explained by other factors than prereceptoral stray light or light passing between cones. The high contrast also leaves no room for an important contribution from deep layers behind the photoreceptors at this wavelength, unless this light is a component of the relatively narrow distribution exiting each cone.

If almost all the light observed in the images is indeed guided light, and we invoke the reversibility of receptor optics, then the light distribution exiting the cone should match the cone aperture for light incident on the cone. If the cone aperture is also narrow for incident light then a relatively large proportion of incident photons pass unguided between the foveal cones. This is consistent with the narrow cone apertures estimated from psychophysical experiments with interference fringes (MacLeod *et al.*, 1992; Chen *et al.*, 1993). One consequence of this is that the transduction efficiency of the foveal cone mosaic is actually less than that expected from the commonly made assumption that the inner segment area is the cone aperture. That the fovea would waste photons in this way is surprising, but its specialty is vision at high light levels where photon catch is relatively unimportant.

Even the best cone images have a mottled appearance, indicating that the efficiency with which light is returned from individual cones varies from receptor to receptor. In power spectra of the cone images, this variability probably contributes to the presence of considerable power at other spatial frequencies than those corresponding to the cone mosaic (see Figs 5 and 7). Whether these differences arise from differences in the antenna properties of individual cones, or perhaps spatial variations in the layer(s) responsible for reflecting the light, is not known.

The clearest evidence for rings in the power spectra was obtained just off the foveal center at about 0.5 deg. We have not yet found convincing evidence for a ring at the foveal center where cone spacing is smallest, and our simulations suggest that this is a limitation imposed by the eye's optics. However, given the small number of subjects we tested and the large individual differences in optical quality that exist, it would not be surprising if subjects could be found in which even the mosaic at the foveal center could be resolved. Our simulations suggest that rods, which have about the same dimensions as foveal cones, are probably equally difficult to resolve. We therefore speculate that the bright spots we have observed at locations containing rods mainly arise from cones. Surprisingly, rings were also less frequently observed at larger eccentricities, such as 2.5 deg. We have not yet succeeded in obtaining convincing evidence for photoreceptors at larger eccentricities despite the fact that cone size and spacing continue to grow while the optical quality of the eye declines more slowly over this range of retinal locations (Jennings & Charman, 1981; Navarro *et al.*, 1993; Williams *et al.*, in press). One

possibility is that the thickening of the inner retina with distance from the center of the foveal pit may reduce the visibility of the receptors. The retina is thickest at the edge of the foveal pit, about 2.5 deg (Polyak, 1957), at which point the visibility of the bright spots has declined considerably. Alternatively, extrafoveal cones may have different reflection properties than those in the fovea. Unlike foveal cones, extrafoveal cones are not inserted into the pigment epithelium (Polyak, 1957), which may reduce the amount of light reflected back through them.

Implications for the optical quality of the eye and retinal sampling

The use of a large exit pupil to image cones near the foveal center may seem to contradict the common view that retinal image quality is best for 2–3 mm pupils, declining at larger pupils due to aberrations in the eye. However, estimates of the eye's modulation transfer function hint that this decline occurs only at low spatial frequencies, and that high frequencies are actually better imaged with large pupils than with small ones (Campbell & Green, 1965; Campbell & Gubisch, 1966). However, the MTFs in these studies are not measured at high enough spatial frequencies to see this effect clearly at larger pupil sizes. Figure 11 shows MTFs for the human eye with a 2 and 6 mm pupil, and an illuminating wavelength of 555 nm. Each MTF is the average of 14 observers measured with the Hartmann–Shack wavefront sensor. The diffraction-limited MTF for a 6 mm pupil is also shown. In the range of spatial frequencies 0–50 c/deg, the MTF for the 6 mm pupil lies below that for a 2 mm pupil, but at 50 c/deg the curves cross. The MTF for the 6 mm pupil continues all the way out to the diffraction limit at 189 c/deg.

The smallest cones we have resolved with confidence in an individual image (subject MM) have a spacing of about 3.5 μm, corresponding to a sampling frequency of 86 c/deg. The smallest cone spacing we have resolved so far using the average power spectrum technique is about 3.0 μm, corresponding to a cone mosaic sampling frequency of about 100 c/deg. However, the power spectra reveal evidence for still higher spatial frequencies in the images, containing power significantly above the system noise out to 150 c/deg. This can be seen in Figs 5 and 7 which show the power leveling off at the noise floor at about 150 c/deg. There is also some psychophysical confirmation: one of us (DW) has observed aliasing within 0.4 deg of the foveal center while viewing a high contrast 90 c/deg grating through a 5 mm natural pupil.

Though the modulation transfer is quite low at high spatial frequencies, information about fine retinal structures is present in the retinal image. The recovery of this information depends on not only the MTF, but also the eye's phase transfer function (PTF). The PTF describes the relative phase shifts introduced by the eye's optics between the spatial frequency components that form the retinal image. The PTF of the eye can sometimes be even more important than the MTF in determining the eye's image-formation capability. For example, the compactness and excellent imaging properties of JL's PSF are largely due to the relative absence of phase shifts in his PTF, while the extended and complex shape of OP's PSF results largely from the presence of phase shifts.

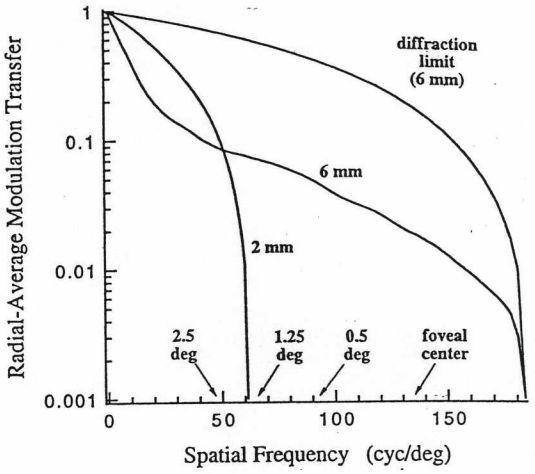

FIGURE 11. Radial-average MTFs for an average human eye with a 2 and 6 mm pupil, and an illuminating wavelength of 555 nm. The radial-average MTFs are the average of 14 observers measured with the Hartmann–Shack wavefront sensor. The diffraction-limited MTF for a 6 mm pupil is also shown. Note the semilog ordinate, chosen to emphasize the high spatial frequency region of the MTFs.

Our MTF measurements imply that, using a large pupil, one can image conventional gratings (i.e., not interference fringes) on the retina with spatial frequencies at least as high as the cone sampling frequency everywhere in the retina. This easily meets the first requirement for producing aliasing, namely that the retinal image contain spatial frequencies exceeding half the sampling frequency, the Nyquist frequency. It is therefore merely a question of whether the contrast is sufficient for aliasing to be visible. Given that the sampling rates of neural arrays beyond the receptors, such as ganglion cells, are even lower than those of cones in the peripheral retina, the possibility that aliasing would intrude in normal vision might seem high. A number of studies have confirmed that aliasing can be seen while viewing conventional gratings (Smith & Cass, 1987; Anderson & Hess, 1990; Galvin & Williams, 1992; Artal *et al.*, 1995).

Despite these experimental observations, which are usually made with optimal stimulus conditions and an optimal refractive state, aliasing is of little or no consequence for normal vision of ordinary scenes (Williams *et al.*, in press). The absence of aliasing in everyday vision suggests that the optical quality of the eye is actually not so badly matched to retinal sampling in peripheral vision, given that the eye is not generally optimally focused and we are rarely confronted with the high contrast patterns required to produce aliasing in the laboratory. Snyder *et al.* (1986, 1990) argued that it is advantageous for optical quality to exceed the limits set by retinal sampling. Considering the subtlety of aliasing phenomena even when viewed under optimal conditions

with laser interferometry, perhaps we should be less surprised that the optical cutoff frequency in the peripheral retina exceeds the retinal sampling limits than that evolution has not provided us with better retinal image quality in the fovea. Though increasing foveal retinal image quality would not increase acuity due to the limit set by the receptor grain, it would probably improve contrast sensitivity before aliasing became visually troublesome in ordinary environments.

Implications for fundus imaging

Most techniques for fundus imaging employ a relatively small exit pupil, typically 2–3 mm, because, for macroscopic retinal features, this yields the best image quality. If an exit pupil were used that approached the size of the dilated pupil, diffraction would introduce a modest loss in image contrast even at microscopic spatial scales, but the eye's aberrations would become severe. These aberrations include not only defocus and astigmatism, which are relatively easy to correct with conventional methods, but also significant higher order aberrations such as coma and spherical aberration (Charman, 1991; Liang & Williams, 1995). Adaptive optics (Tyson, 1991), in which a deformable mirror is shaped to compensate for the aberrations in a particular eye (Dreher *et al.*, 1989), provides a promising way to achieve diffraction-limited fundus imaging through a dilated pupil, particularly since it is now possible to measure the eye's wave aberration with an automated wavefront sensor (Liang *et al.*, 1994; Liang & Williams, 1995). Our success in resolving the cone photoreceptors in eyes with relatively few higher order aberrations suggests that adaptive optics may make it possible, in normal eyes, to visualize many features of the living human retina on a microscopic spatial scale.

REFERENCES

Anderson, S. J. & Hess, R. F. (1990). Post-receptoral undersampling in normal human peripheral vision. *Vision Research*, *30*, 1507–1515.

Artal, P., Derrington, A. M. & Colombo, E. (1995). Refraction, aliasing, and the absence of motion reversals in peripheral vision. *Vision Research*, *35*, 939–947.

Artal, P. & Navarro, R. (1989). High-resolution imaging of the living human fovea: Measurement of the intercenter cone distance by speckle interferometry. *Optics Letters*, *14*, 1098–1100.

van Blokland, G. J. (1986). Directionality and alignment of the foveal receptors, assessed with light scattered from the human fundus *in vivo*. *Vision Research*, *26*, 495–500.

van Blokland, G. J. & van Norren, D. (1986). Intensity and polarization of light scattered at small angles from the human fovea. *Vision Research*, *26*, 485–494.

Burns, S. A., Wu, S., Elsner, A. E. & Delori, F. (1995). Reflectometric measurement of human cone photoreceptor directionality. *Vision Science and its Applications*, 1995 OSA Technical Digest Series (Optical Society of America, Washington, DC), *1*, 102–105.

Campbell, F. W. & Green, D. G. (1965). Optical and retinal factors affecting visual resolution. *J. Physiology (London)*, *181*, 576–593.

Campbell, F. W. & Gubisch, R. W. (1966). Optical quality of the human eye. *J. Physiology (London)*, *186*, 558–578.

Charman, W. N. (1991). Optics of the human eye. *Vision and Visual Dysfunction*, *1*, 1–26.

Chen, B., Makous, W. & Williams, D. R. (1993). Serial spatial filters in vision. *Vision Research*, *33*, 413–427.

Curcio, C. A., Sloan, K. R., Kalina, R. E. & Hendrickson, A. E. (1990). Human photoreceptor topography. *J. Comparitive Neurology*, *292*, 497–523.

Dainty, J. C. (1984). Stellar speckle interferometry. In Dainty, J. C. (Ed.), *Laser speckle and related phenomena* (pp. 255–320). New York: Springer-Verlag.

Dreher, A. W., Bille, J. F. & Weinreb, R. N. (1989). Active optical depth resolution improvement of the laser tomographic scanner. *Applied Optics*, *28*, 804–808.

Galvin, S. J. & Williams, D. R. (1992). No aliasing at edges in normal viewing. *Vision Research*, *32*, 2251–2259.

Gorrand, J. & Delori, F. (1995). A reflectometric technique for assessing photoreceptor alignment. *Vision Research*, *35*, 999–1010.

Helmholtz, H. (1873). *Popular lectures on scientific subjects* (Atkinson, E. Trans., p. 227). New York: D. Appleton and Company.

Jagger, W. S. (1985). Visibility of photoreceptors in the intact living cane toad eye. *Vision Research*, *25*, 729–731.

Jennings, J. A. M. & Charman, W. N. (1981). Off-axis image quality in the human eye. *Vision Research*, *21*, 445–455.

Krauskopf, J. (1965). Some experiments with a photoelectric ophthalmoscope. In Bouman, M. A. & Vos, J. J. (Eds), *Excerpta Medica International Congress Series, No. 125*. Amsterdam: Excerpta Medica Foundation.

Land, M. F. (1990). Direct observation of receptors and images in simple and compound eyes. *Vision Research 30*, 1721–1734.

Land, M. F. & Snyder, A. W. (1985). Cone mosaic observed directly through natural pupil of live vertebrate. *Vision Research*, *25*, 1519–1523.

Liang, J., Grimm, B., Goelz, S. & Bille, J. F. (1994). Objective measurement of wave aberrations of the human eye with the use of a Hartmann–Shack wave-front sensor. *Journal of the Optical Society of America, A*, *11*, 1949–1957.

Liang, J. & Williams, D. R. (1995). Effect of higher order aberrations on image quality in the human eye. *Vision Science and its Applications*, 1995 OSA Technical Digest Series (Optical Society of America, Washington, DC), *1*, 70–73.

Lowenthal, S. & Joyeux, D. (1971). Speckle removal by a slowly moving diffuser associated with a motionless diffuser. *Journal of the Optical Society of America, 61, 847–851.*

MacLeod, D. I. A., Williams, D. R. & Makous, W. (1992). A visual nonlinearity fed by single cones. *Vision Research*, *32*, 347–363.

Navarro, R., Artal, P. & Williams, D. R. (1993). Modulation transfer of the human eye as a function of retinal eccentricity. *Journal of the Optical Society of America, A*, *10*, 201–212.

Polyak, S. (1957). *The vertebrate visual system* (pp. 261, 264, 266). Chicago: University of Chicago Press.

Smith, R. A. & Cass, P. R. (1987). Aliasing in the parafovea with incoherent light. *Journal of The Optical Society of America, A*, *4*, 1530–1534.

Snyder, A. W. (1979). The physics of compound eyes. In Autrum, H. (Ed.), *Vol. VII/6A Handbook of sensory physiology.* (pp. 225–313). New York: Springer-Verlag.

Snyder, A. W., Bossomaier, T. J., & Hughes, A. (1986). Optical image quality and the cone mosaic. *Science*, *231*, 499–501.

Snyder, A. W., Bossomaier, T. J. & Hughes, A. (1990). The theory of comparative eye design. In Blakemore, C. (Ed.), *Vision: Coding and efficiency* (pp. 46–47). Cambridge: Cambridge University Press.

Snyder, A. W. & Miller, W. H. (1977). Photoreceptor diameter and spacing for highest resolving power. *Vision Research*, 67, 696–698.

Tyson, R. K. (1991). *Principles of adaptive optics*. San Diego: Academic Press, Inc.

Walsh, G., Charman, W. N. & Howland, H. C. (1984). Objective technique for the determination of monochromatic aberrations of the human eye. *Journal of The Optical Society of America, A*, *1*, 987–992.

Wehner, R. (1981). Spatial vision in arthropods. In Autrum, H. (Ed.), *Handbook of sensory physiology* (Vol. VII/6C, pp. 297–311). New York: Springer-Verlag.

Williams, D. R. (1985). Aliasing in human foveal vision. *Vision Research*, *25*, 195–205.

Williams, D. R. (1988). Topography of the foveal cone mosaic in the living human eye. *Vision Research*, *28*, 433–454.

Williams, D. R. (1992). Photoreceptor sampling and aliasing in human vision. In Moore, D. T. (Ed), *Tutorials in Optics* (pp. 15–28). Washington: Optical Society of America.

Williams, D. R., Artal, P., Navarro, R., McMahon, M. J. & Brainard, D. H. (1996). Off-axis optical quality retinal sampling in the human eye. *Vision Research*, (in press).

Yellott, J. I. Jr (1982). Spectral analysis of spatial sampling by photoreceptors: Topological disorder prevents aliasing. *Vision Research*, *22*, 1205–1210.

Yellott, J. I. Jr (1983). Spectral consequences of photoreceptor sampling in the rhesus retina. *Science*, *221*, 382–385.

Zwick, H., Lund, D. J., Elliot, R. & Schuschereba, S. T. (1995). Confocal spectral ophthalmoscopic imaging of retinal laser damage in small vertebrate eyes. In Parel, M., Ren, Q. & Joos, K. M. (Eds), *Ophthalmic technologies V, Proceedings of the Society of Photo-Optical Instrument Engineering 2393* (pp. 182–188).

Acknowledgements—This research was supported by NIH Grants EY04367, EY01319 and a RE & HPB Fellowship. Research was also supported in part by the Center for Electronic Imaging Systems. We extend a special thanks to Al Russell, Bill Haake, and Andrew Asproulis for technical assistance in the construction of the fundus camera and to Rafael Navarro and Pablo Artal for helpful discussions.